Available online at www.sciencedirect.com
SCIENCE DIRECT®
Surface Science 553 (2004) 23–29
SURFACE SCIENCE
www.elsevier.com/locate/susc

Auger electron spectroscopy investigation of SO_2/Zr(0 0 0 1)

N. Stojilovic, J.C. Tokash, R.D. Ramsier *

Departments of Physics, Chemistry, and Chemical Engineering, The University of Akron, 250 Buchtel Commons, Ayer Hall 111, Akron, OH 44325-4001, USA

Received 19 November 2003; accepted for publication 4 February 2004

Abstract

The adsorption of SO_2 on Zr(0 0 0 1) at 150 K has been investigated under ultrahigh vacuum (UHV) conditions. Auger electron spectroscopy (AES) reveals saturation of both sulfur and oxygen signals at exposures of about 1 Langmuir (L). Changes in the overlapping Zr(MNV) + S(LMM) feature as well as in the Zr(MNN) feature are discussed. In particular, the Zr(MNN) feature changes with both exposure and annealing history, complicating the identification of sulfur using Auger peak-to-peak height ratios. We propose that SO_2 dissociates on Zr(0 0 0 1) under these conditions, since no thermal desorption of sulfur dioxide is detected for exposures up to 5 L. However, the desorption of small quantities of 34 and 32 amu species near 250 K is observed by temperature programmed desorption (TPD) measurements. Integrated desorption peak areas of these species saturate near 1 L, consistent with the saturation behavior observed by AES. Electron bombardment (500 eV) reduces H_2S desorption presumably by removing surface hydrogen via electron stimulated mechanisms, but has no effect on Auger spectra.

Keywords: Zirconium; Sulphur; Auger electron spectroscopy; Thermal desorption

1. Introduction

Sulfur is a well-known poison for surface catalysis. Like many metals, zirconium holds impurity sulfur, which can segregate and influence the surface kinetics of this reactive metal [1,2]. Unlike oxygen and carbon that upon annealing diffuse into the bulk, sulfur segregates to the surface after prolonged annealing at high temperatures [3,4]. For instance, the influence of surface sulfur on oxygen adsorption on zirconium surfaces has been investigated previously. It was reported that segregation of sulfur from the bulk delays surface oxidation [1]. In another study, sulfur segregation to the surface resulted in a decreased sticking coefficient of oxygen and a shift of the Zr(MNV, 147 eV) Auger electron feature to 152 eV [2].

The behavior of oxygen on zirconium surfaces has been investigated in various studies [1–11]. For instance, in an investigation of $^{18}O_2$ on Zr(0 0 0 1) [5], kinetic mixing of adsorbed oxygen with subsurface species was observed. In the same study, the thermal desorption of water was detected with even more $H_2{}^{16}O$ than $H_2{}^{18}O$. Both theoretical [6] and experimental [7–9] findings reveal that oxygen occupies octahedral holes in the Zr(0 0 0 1) subsurface region. Thus, this isotopic mixing can

* Corresponding author. Tel.: +1-330-972-4936; fax: +1-330-972-6918.
E-mail address: rex@uakron.edu (R.D. Ramsier).

0039-6028/$ - see front matter © 2004 Published by Elsevier B.V.
doi:10.1016/j.susc.2004.02.002

be explained by mass transport during heating. On the other hand, studies of the interaction of sulfur containing species with zirconium surfaces are rare. In one study of room temperature adsorption of H_2S on Zr(0 0 0 1) it was found that surfaces with high sulfur content do not adsorb oxygen in detectable amounts [10].

Following adsorption on most metal surfaces, SO_2 dissociates either spontaneously or thermally with no molecular desorption. However, molecular desorption has been observed from noble metal surfaces such as Ag(1 1 1) [12,13] and Ag(1 1 0) [12,14]. To our knowledge this is the first investigation of SO_2 adsorption on zirconium surfaces under ultrahigh vacuum (UHV) conditions. The fact that Auger electron spectroscopy (AES) Zr(MNV) and S(LMM) features overlap makes these studies difficult but also important. In this paper, we focus on changes in Auger features induced by the adsorption of SO_2 on Zr(0 0 0 1) at 150 K, and track these as a function of exposure and annealing temperature. Additionally we discuss 34 and 32 amu temperature programmed desorption (TPD) features, the effect of electron bombardment, and probe the surface structure with low energy electron diffraction (LEED) methods.

2. Experiment

The Zr(0 0 0 1) single crystal (99.99% purity) used in this study has a cylindrical shape with a radius of 3 mm and a thickness of 1 mm. The crystal is polished to 30 nm particle size with an uncertainty in orientation less than 1°. By using tantalum wires spot-welded to the sample direct current heating of the crystal is performed. As part of a temperature-control feedback loop two thermocouples are also spot-welded to the crystal. The sample cooling is performed by means of a copper braid connected to a liquid-nitrogen cold finger.

Four-grid retarding-field AES (3 keV, 15 $\mu A\,cm^{-2}$) and LEED (60 eV, 2 $\mu A\,cm^{-2}$) data indicated that attaining "clean" Zr(0 0 0 1) surfaces, characterized by C(KLL)/Zr(MNN) $\sim$ 0.21, O(KLL)/Zr(MNN) $\sim$ 0.15 and [Zr(MNV) + S(LMM)]/Zr(MNN) $\sim$ 0.91 [15], required several sputtering cycles (Ar^+, 2 keV, 2 $\mu A\,cm^{-2}$) followed by annealing to 840 K for 2 min. After cleaning, the base pressure at which experiments were conducted was 4×10^{-10} Torr or lower. SO_2 gas (Matheson, 99.98%) was introduced into the UHV system through a stainless steel gas-handling manifold. More detailed descriptions of the UHV system were reported previously [16,17]. The heating rate during TPD and stepwise annealing experiments was 1.8 K/s. Mass-to-charge values during TPD and backfilling are monitored by the quadrupole mass spectrometer (QMS). The QMS was positioned in line-of sight with respect to the sample surface. AES and LEED data were collected at the 150 K adsorption temperature.

3. Results and discussion

3.1. AES

Fig. 1 shows Auger electron spectra of a "clean" zirconium surface, after exposure to 3.4 L of SO_2 at 150 K, and after annealing to 850 K. The presence of carbon and oxygen in "clean" surface spectra is not uncommon for this gettering material, as seen in the bottom spectrum of Fig. 1. After SO_2 adsorption the Zr(MNV) and S(LMM) features overlap making sulfur detection difficult. Note that SO_2 adsorption results in a decrease of the C(KLL) and all the Zr Auger features except the Zr(MNV) because it overlaps with S(LMM). The decrease in the Zr and C features is due to electron attenuation by S and O atoms.

In Fig. 1 also note an increase in the O(KLL) feature after SO_2 adsorption. Annealing to 850 K removes surface oxygen but on the other hand results in even greater sulfur content as can be seen from an increase in Zr(MNV) + S(LMM) feature. Since no desorption of oxygen-containing species at higher temperatures is observed in TPD we conclude that oxygen diffuses into the bulk. Although we observe a small amount of 32 amu desorption near 250 K it is not possible to distinguish whether this TPD signal comes from oxygen or from sulfur in these experiments. Oxygen diffusion into the bulk was observed previously for nitric oxide [17], water [18], and methanol [19] on

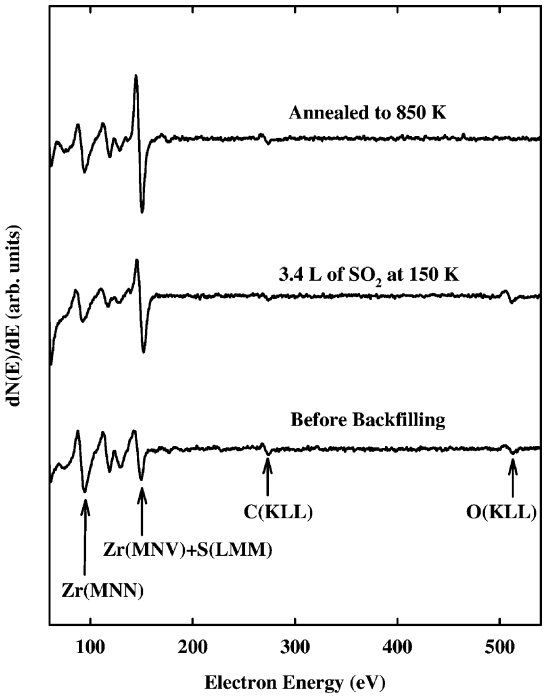

Fig. 1. Auger electron spectra recorded before backfilling, after 3.4 L SO_2 exposure, and after annealing to 850 K. All spectra are collected near 150 K.

Zr(0 0 0 1) surfaces. In the present case, even though a significant amount of sulfur resides in the near-surface region at high annealing temperatures it does not block oxygen diffusion into the crystal lattice, in agreement with oxygen behavior in these other studies [17–19]. This is interesting since sulfur is a relatively large atom. We conclude that zirconium has a high affinity for taking oxygen into solid solution even when a significant amount of sulfur is present in the near-surface region.

Fig. 2 shows changes in the normalized Zr(MNV) + S(LMM) Auger feature versus annealing temperature for three SO_2 exposures. Following exposures of 0.4 L (Fig. 2A), 1.1 L (Fig. 2B), and 3.7 L (Fig. 2C) the peak-to-peak height of this feature changes in the same fashion with stepwise annealing. At about 1 L saturation occurs and it is difficult to distinguish between the 1.1 L and 3.7 L data sets of Fig. 2. It should be stressed that the Zr(MNV) feature is considered to be the most affected by chemisorption since it involves valence

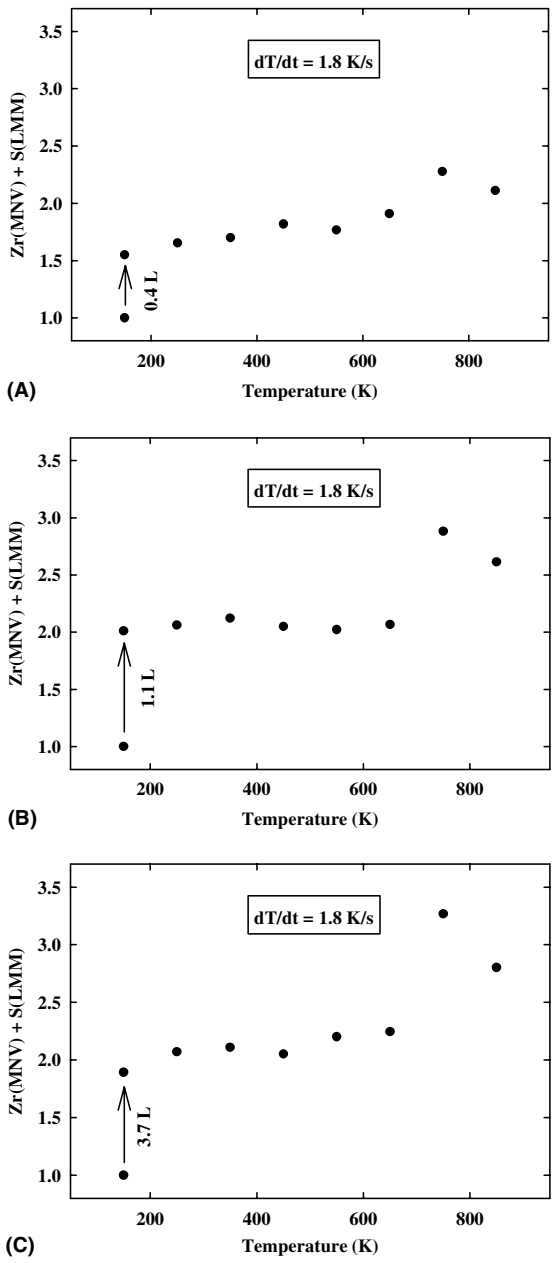

Fig. 2. Peak-to-peak heights of the convoluted Zr(MNV) + S(LMM) Auger features following SO_2 exposures of 0.4 L (A), 1.1 L (B), and 3.7 L (C), versus annealing temperature. The uncertainty in the measurements is on the order of the size of the data points.

electrons [3]. However, as a result of overlap with the S(LMM) energy, a convoluted feature is

observed. An interesting observation is that almost no change in the Zr(MNV) + S(LMM) feature is observed for stepwise annealing until 700 K. Annealing to 700 K results in an increase of the convoluted feature regardless of exposure. This is most likely due to oxygen diffusion into the crystal and its replacement by sulfur at higher temperatures.

Now we consider the Zr(MNN) Auger feature that is typically assumed to be much less affected by adsorbed species [3]. In Fig. 3 the normalized peak-to-peak heights of the Zr(MNN) Auger features are plotted as a function of annealing temperature for the same exposures as in Fig. 2. A decrease in the Zr(MNN) feature of about 33% is observed following exposure to 0.4 L of SO_2. Note that unlike the Zr(MNV) + S(LMM) feature, the Zr(MNN) feature changes with 250–650 K annealing. Since AES is capable of probing not only the surface but also the nearby subsurface region, these changes most likely reflect diffusion of atoms into the bulk or the rearrangement of subsurface species.

The Zr(MNN) feature is less sensitive to variations in exposure than the convoluted Zr(MNV) + S(LMM) feature. For example, following 0.4 L of SO_2, the Zr(MNN) signal drops by about 33% compared to the 50% increase in the Zr(MNV) + S(LMM) feature for the same exposure. Note in Fig. 3A that after exposure and annealing to 850 K the peak-to-peak height of the Zr(MNN) feature returns to the "clean" surface value. Since there is no decrease in sulfur content upon annealing we conclude that these changes are caused by oxygen diffusion into the bulk. Comparing this with Fig. 3B and C, we see that at higher exposures the Zr(MNN) feature does not return to its original intensity after annealing to high temperature. Thus, the measured Zr(MNN) Auger electron signal depends on both SO_2 exposure and annealing history.

Fig. 4 shows [Zr(MNV) + S(LMM)]/Zr(MNN) Auger peak-to-peak height (APPH) ratios calculated from the data of Figs. 2 and 3. The figure reveals how the APPH ratio changes as a function of exposure and annealing temperature. The APPH ratios follow the trends seen in Fig. 2. We expect this since the increase in the Zr(MNV) + S(LMM) feature due to SO_2 adsorption is more pronounced than the decrease in the Zr(MNN) feature. A significant increase in the APPH ratio is

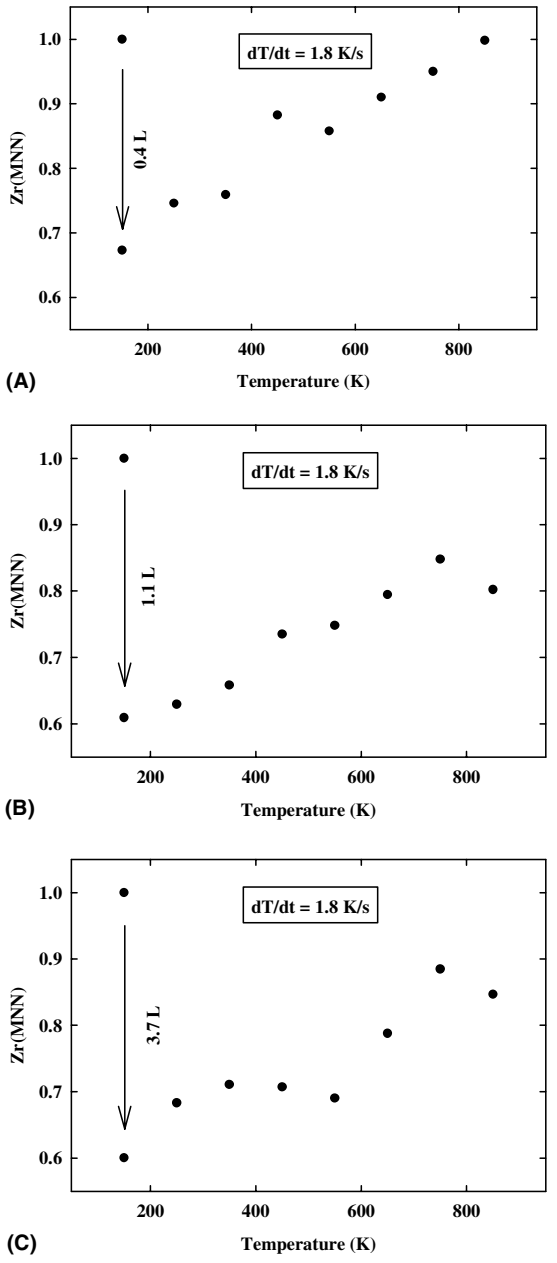

Fig. 3. Peak-to-peak heights of the Zr(MNN) Auger features following SO_2 exposures of 0.4 L (A), 1.1 L (B), and 3.7 L (C), versus annealing temperature. The uncertainty in the measurements is on the order of the size of the data points.

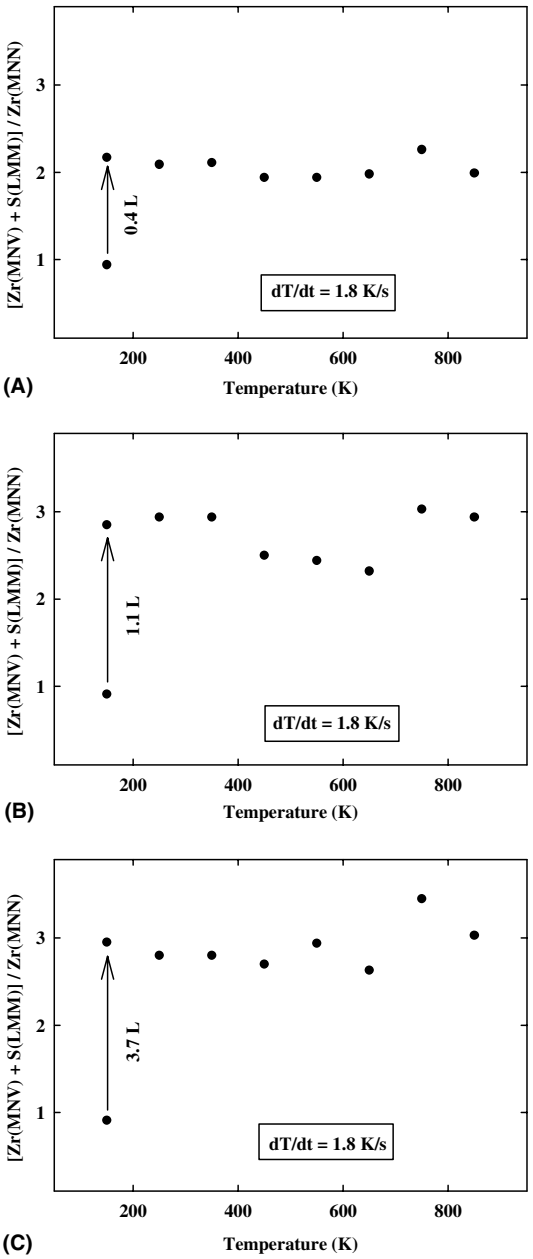

Fig. 4. The [Zr(MNV) + S(LMM)]/Zr(MNN) APPH ratios following SO_2 exposures of 0.4 L (A), 1.1 L (B), and 3.7 L (C), versus annealing temperature. These data are calculated from those in Figs. 2 and 3.

observed following exposure of Zr(0 0 0 1) to SO_2. Annealing to 650 K does not affect the APPH ratio significantly. However, since the Zr(MNN) feature changes with respect to both exposure and annealing temperature, we propose that relying on only APPH ratios may be misleading. For example, looking at the APPH ratios only does not reveal that there is more sulfur in the near-surface region after high-temperature annealing than there is immediately after adsorption.

Figs. 5 and 6 show how the [Zr(MNV) + S(LMM)]/Zr(MNN) and O(KLL)/Zr(MNN) ratios, respectively, change with exposure. Note the rapid increase in APPH ratios in both figures and saturation near 1 L. Saturation at relatively low exposure can be rationalized by the presence of

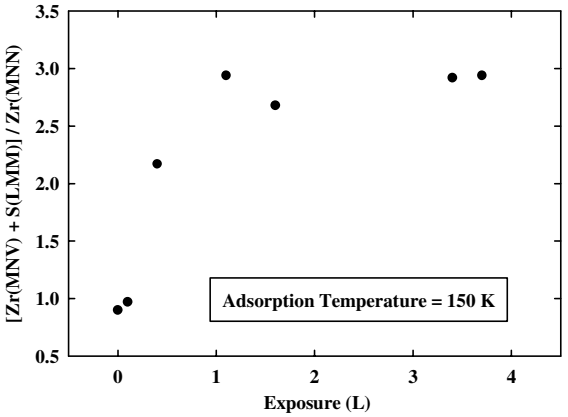

Fig. 5. The [Zr(MNV) + S(LMM)]/Zr(MNN) ratio versus SO_2 exposure at 150 K.

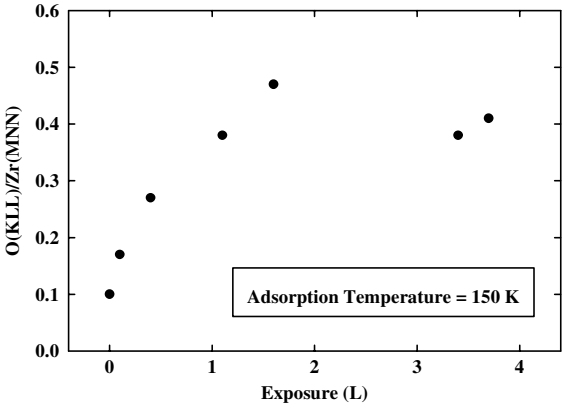

Fig. 6. The O(KLL)/Zr(MNN) ratio versus SO_2 exposure at 150 K.

sulfur that is known to reduce the sticking coefficient. However, these changes do not only reflect the contributions of sulfur and oxygen species. Namely, the denominator is also changing making interpretation of APPH data tenuous. Typically, such ratios are used to track adsorbate species. However, in the case of Zr, surface–subsurface diffusion plays an important role in the evolution of Auger features. Recall that Fig. 3 clearly shows that the Zr(MNN) feature exhibits different behavior depending on the SO_2 exposure and annealing temperature. It should be noted here that 500 eV electron bombardment up to fluences of 10^{17} cm^{-2} had no effect on the AES data collected in this study.

3.2. TPD

No desorption of SO_2 is observed in our TPD experiments. Since AES reveals the presence of both sulfur and oxygen, SO_2 dissociates either during adsorption or subsequent heating. On the other hand, desorption of 32 and 34 amu species is detected near 250 K. Fig. 7 shows H_2S (34 amu) desorption following SO_2 adsorption at 150 K. Desorption of atomic sulfur from metals has previously been reported [20,21] and in principle the 32 and 34 amu signals could be attributed to the two sulfur isotopes. Note that the integrated desorption yields exhibit saturation behavior above 1 L exposures, as shown in Fig. 8. This provides more evidence that dissociative SO_2 adsorption at 150 K reduces the sticking coefficient. We therefore propose that the AES ratios shown in Figs. 5 and 6 do indeed correspond to surface saturation.

It should be pointed out that the amount of desorbing species is very small. This can be inferred from the signal to noise ratios in the spectra of Fig. 7, and is reflected in the uncertainty bars of Fig. 8. Obviously, there must be a source of hydrogen for the production of H_2S, and we propose that the subsurface region is responsible. Zirconium getters hydrogen, which is known to be attracted from the bulk to the surface in the presence of adsorbed oxygen [22]. We propose that after dissociation of SO_2 and migration of hydrogen to the surface, adsorbed sulfur reacts with hydrogen to desorb as H_2S. We find that 500 eV electron bombardment reduces the amount of H_2S

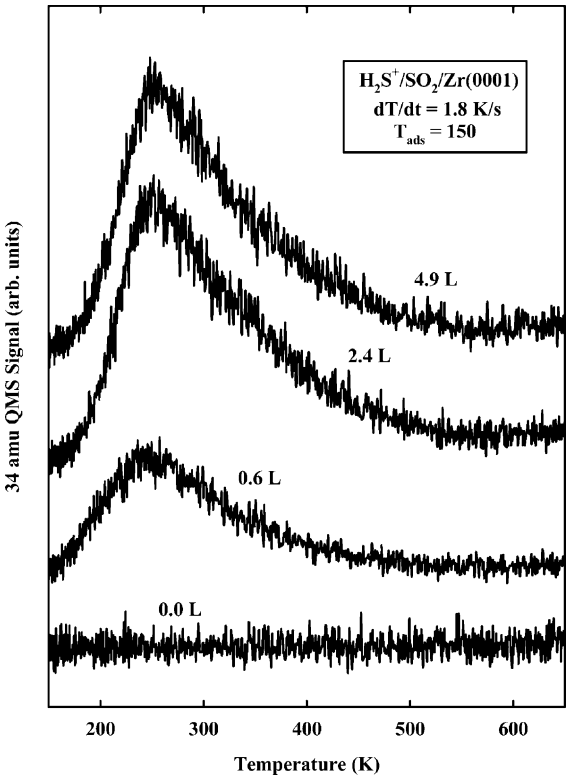

Fig. 7. H_2S^+ (34 amu) thermal desorption spectra following 150 K SO_2 adsorption on Zr(0 0 0 1) surfaces.

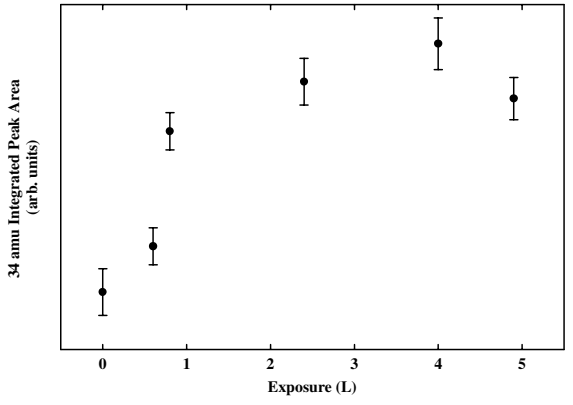

Fig. 8. Integrated 34 amu thermal desorption peak areas versus SO_2 exposure.

desorption, most likely by removing surface hydrogen via electron stimulated desorption [23].

3.3. LEED

The absence of superstructure LEED patterns is not uncommon for SO_2 adsorbed on various metal surfaces. It is known that electron beams easily destroy an ordered layer [24] thus making LEED analysis difficult, if not impossible. LEED patterns (not shown) of SO_2/Zr(0 0 0 1) imply that dissociation fragments randomly orient since we have no evidence for ordered structures for a variety of exposures. High-temperature annealing removes oxygen via diffusion into the bulk and a diffuse 1×1 pattern is reestablished. The disordered adsorbed layer at 150 K is most likely due to the presence of both sulfur and oxygen. However, we do not know the effects of the small amount of surface carbon. It is interesting to compare our SO_2/Zr(0 0 0 1) surfaces with those of H_2S/Zr-(0 0 0 1) [10]. There, LEED intensity analysis revealed that annealing to 873 K formed a stable (3×3) surface structure. However, we were not able to detect any ordered structures by LEED in our annealing experiments for various exposures.

4. Summary

Following adsorption at 150 K, the interaction of SO_2 with Zr(0 0 0 1) has been investigated. After adsorption AES reveals an increase in both the S(LMM) and O(KLL) features as expected, with saturation at about 1 L. The thermal desorption of 32 and 34 amu species is detected in small quantities near 250 K with yields that also saturate near 1 L. High-temperature annealing causes oxygen diffusion into the bulk and the peak-to-peak height of the S(LMM) feature correspondingly increases. This demonstrates the complicated thermal behavior of the zirconium system, and the role of mass transport between the surface and subsurface regions [25]. Interestingly, the Zr(MNN) feature also depends on SO_2 exposure and annealing history. We therefore demonstrate that the [Zr(MNV) + S(LMM)]/Zr(MNN) AES peak-to-peak height ratio by itself may not accurately represent the cleanliness of Zr surfaces with respect to sulfur.

Acknowledgements

Acknowledgement is made to the Donors of the American Chemical Society Petroleum Research Fund for partial support of this research.

References

[1] T. Tanabe, M. Tomita, Surf. Sci. 220 (1989) 333.
[2] K. Ojima, K. Ueda, Appl. Surf. Sci. 165 (2000) 141.
[3] J.S. Foord, P.J. Goddard, R.M. Lambert, Surf. Sci. 94 (1980) 339.
[4] G.B. Hoflund, G.R. Corallo, D.A. Asbury, R.E. Gilbert, J. Vac. Sci. Technol. A 5 (1987) 1120.
[5] Y.C. Kang, R.D. Ramsier, Appl. Surf. Sci. 195 (2002) 196.
[6] M. Yamamoto, C.T. Chan, K.M. Ho, S. Naito, Phys. Rev. B 54 (1996) 14111.
[7] Y.M. Wang, Y.S. Li, K.A.R. Mitchell, Surf. Sci. 343 (1995) L1167.
[8] Y.M. Wang, Y.S. Li, K.A.R. Mitchell, Surf. Sci. 342 (1995) 272.
[9] C.-S. Zhang, B.J. Flinn, I.V. Mitchell, P.R. Norton, Surf. Sci. 245 (1991) 373.
[10] P.C. Wong, K.A.R. Mitchell, Can. J. Chem. 64 (1986) 2409.
[11] P.C. Wong, K.A.R. Mitchell, Can. J. Phys. 65 (1987) 464.
[12] J. Ahner, A. Effendy, K. Vajen, H.-W. Wassmuth, Vacuum 41 (1990) 98.
[13] M.E. Castro, J.M. White, J. Chem. Phys. 95 (1991) 6057.
[14] D.A. Outka, R.A. Madix, Surf. Sci. 137 (1984) 242.
[15] N. Stojilovic, Y.C. Kang, R.D. Ramsier, Surf. Interface Anal. 33 (2002) 945.
[16] Y.C. Kang, M.M. Milovancev, D.A. Clauss, M.A. Lange, R.D. Ramsier, J. Nucl. Mater. 281 (2000) 57.
[17] Y.C. Kang, R.D. Ramsier, J. Nucl. Mater. 303 (2002) 125.
[18] S. Ankrah, Y.C. Kang, R.D. Ramsier, J. Phys.: Condens. Matter 15 (2003) 1899.
[19] N. Stojilovic, D.W. Weber, R.D. Ramsier, Appl. Surf. Sci. 218 (2003) 188.
[20] C. Park, H.M. Kramer, E. Bauer, Surf. Sci. 116 (1982) 467.
[21] H. Gutleben, E. Bechtold, Surf. Sci. 191 (1987) 157.
[22] D.A. Asbury, G.B. Hoflund, W.J. Peterson, R.E. Gilbert, R.A. Outlaw, Surf. Sci. 185 (1987) 213.
[23] R.D. Ramsier, J.T. Yates Jr., Surf. Sci. Rep. 12 (1991) 243.
[24] P. Zebisch, M. Weinelt, H.-P. Steinruck, Surf. Sci. 295 (1993) 295.
[25] Y.C. Kang, R.D. Ramsier, Surf. Sci. 519 (2002) 229.